From Organometallic Zinc and Copper Complexes to Highly Active Colloidal Catalysts for the Conversion of CO2 to Methanol

Neil J. Brown,[†] Andrés García-Trenco,[†] Jonathan Weiner,[†] Edward R. White,[†] Matthew Allinson,[†] Yuxin Chen,[†] Peter P. Wells,[‡,§] Emma K. Gibson,[‡,§] Klaus Hellgardt,[⊥] Milo S. P. Shaffer,*,[†] and Charlotte K. Williams*,[†]

[†]Department of Chemistry, Imperial College London, South Kensington, London SW7 2AZ, United Kingdom

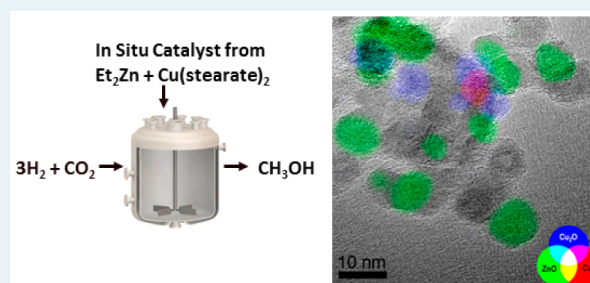[‡]The UK Catalysis Hub, Research Complex at Harwell, Harwell, Oxon OX11 0FA, United Kingdom

[§]Kathleen Lonsdale Building, Department of Chemistry, University College London, Gordon Street, London WC1H 0AJ, United Kingdom

[⊥]Department of Chemical Engineering, Imperial College London, South Kensington, London SW7 2AZ, United Kingdom

Ⓢ Supporting Information

ABSTRACT: A series of zinc oxide and copper(0) colloidal nanocatalysts, produced by a one-pot synthesis, are shown to catalyze the hydrogenation of carbon dioxide to methanol. The catalysts are produced by the reaction between diethyl zinc and bis(carboxylato/phosphinato)copper(II) precursors. The reaction leads to the formation of a precatalyst solution, characterized using various spectroscopic (NMR, UV−vis spectroscopy) and X-ray diffraction/absorption (powder XRD, EXAFS, XANES) techniques. The combined characterization methods indicate that the precatalyst solution contains copper(0) nanoparticles and a mixture of diethyl zinc and an ethyl zinc stearate cluster compound $[Et_4Zn_5(stearate)_6]$. The catalysts are applied, at 523 K with a 50 bar total pressure of a 3:1 mixture of H_2/CO_2, in the solution phase, quasi-homogeneous, hydrogenation of carbon dioxide, and they show high activities (>55 mmol/g_{ZnOCu}/h of methanol). The postreaction catalyst solution is characterized using a range of spectroscopies, X-ray diffraction techniques, and transmission electron microscopy (TEM). These analyses show the formation of a mixture of zinc oxide nanoparticles, of size 2−7 nm and small copper nanoparticles. The catalyst composition can be easily adjusted, and the influence of the relative loadings of ZnO/Cu, the precursor complexes and the total catalyst concentration on the catalytic activity are all investigated. The optimum system, comprising a 55:45 loading of ZnO/Cu, shows equivalent activity to a commercial, activated methanol synthesis catalyst. These findings indicate that using diethyl zinc to reduce copper precursors in situ leads to catalysts with excellent activities for the production of methanol from carbon dioxide.

KEYWORDS: hydrogenation of CO_2, CO_2 reduction, methanol synthesis, colloidal catalysts, Cu-ZnO catalysts, nanoparticles, nanocatalysts, catalysts from organometallic

◼ INTRODUCTION

Using waste CO_2 is a high priority: among the most promising options are the synthesis of polymers and the reduction to alcohols which may serve as fuels.[1] By applying renewable or off-peak power to make hydrogen, for example, via electrolysis of water, it is envisaged that carbon dioxide hydrogenation to methanol could reduce our dependence on fossil fuels.[2] Methanol is an attractive energy vector and a promising renewable transport fuel, particularly because its use is compatible with existing fuels infrastructures.[3] In China, methanol is already being applied, in blends with gasoline, as a fuel.[4]

Methanol is currently produced on a huge scale (>40 million tonnes, globally in 2009), mostly from synthesis gas (CO/H_2), generated by coal gasification or methane reforming, converted using ternary heterogeneous Cu/ZnO/Al_2O_3 catalysts.[5] There
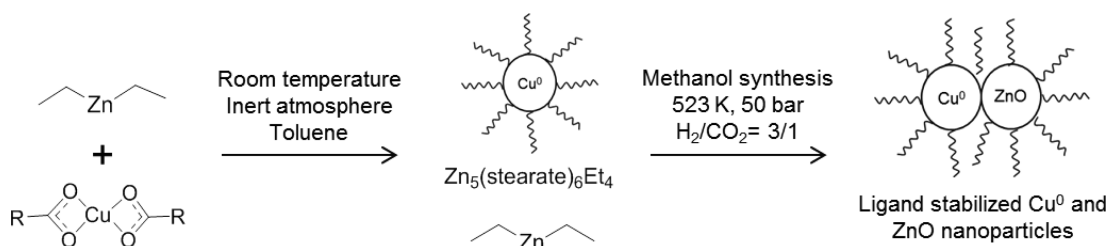
is also a good precedent for these same catalysts to be used for the hydrogenation of carbon dioxide.[3b,6] They are generally prepared by metal salt coprecipitation, following by calcination, aging, nanostructuring, and reduction cycles.[7] Controlling the conditions for these steps is essential to maximize catalyst activity. Detailed investigations indicate that maximizing the ZnO/Cu interface is crucial, through controlling the Zn/Cu loading, introducing a suitable support, and ensuring intimate mixing of the phases, on the nanometre scale.[5e,7] However, current synthesis methods require the preformation of mineral phases, most commonly zincian malachite, which fundamentally limit the loading of Zn/Cu (in the case of zincian

Scheme 1. Representation of the Formation of the Ligand-Stabilized Cu and ZnO Nanoparticles from Diethyl Zinc and Bis(stearate)copper(II) Precursor Using the One-Pot Synthesis Method

malachite, to 3:7) and predetermine the products of aging and, hence, the extent and quality of the interface.[5b] Furthermore, such coprecipitation routes require forcing conditions to decompose the mineral, thereby limiting the nanomorphology of the catalyst. Recent elegant structural studies of these ternary catalysts have revealed that some surface sites are dynamic.[5c−e] For these reasons, there is an impetus to develop new catalyst syntheses.[8] For example, Tsang and co-workers have mixed (in the solid state) isolated nanoparticles of ZnO and Cu to produce high-activity CO_2 hydrogenation heterogeneous catalysts and have correlated activity to exposure of particular crystal facets.[9]

Methanol can also be efficiently produced by slurry phase methods, whereby the active catalyst is dissolved or suspended in a high-boiling solvent (such as squalane).[10] Of particular interest is the use of inorganic/organometallic precursor compounds to produce well-defined, quasi-homogeneous nanoparticles for catalysis. The groups of Fischer and Schüth have pioneered the application of colloidal solutions of nanoparticles (Cu and/or ZnO) as high-activity catalysts for such solution phase syn-gas to methanol processes.[11] Simon et al. reported, as early as 1988 that the reaction between $Cu(acac)_2$ and Et_2Zn in the presence of 1,3-butadiene in an organic solvent formed an efficient syn-gas catalyst system with a high selectivity for ethanol and methanol formation.[12] Corker and Evans used EXAFS to investigate the precatalyst solution. They proposed it comprised a mixture of colloidal copper and an oxozinc cluster compound (of undefined structure and stoichiometry); however, detailed characterization of the cluster and changes to the system during and after catalysis were not carried out.[13]

In the past 10 years, Fischer and co-workers have pioneered various routes to catalytic nanoparticles, including hydro-thermal decomposition, hydrogenolysis, photochemical decomposition, chemical vapor deposition (CVD), and atomic layer deposition (ALD), using organo-Zn and Cu precursors.[11a−q] In 2005, Schüth and co-workers applied trioctyl aluminum reagents as the reductants and ligands for copper nanoparticles; these systems showed high activities for liquid phase methanol catalysis.[11r] Fischer and Muhler have also applied colloidal nanoparticles of ZnO/Cu prepared by hydrothermal decomposition of well-defined inorganic compounds,[11b,g,k,n,p] some of which show excellent activities for the liquid phase synthesis of methanol from syn-gas.[11i] In 2006, they reported a high-activity system prepared by the addition of diethyl zinc to a hot (200 °C) solution of a copper(II) alkoxide precursor. This system formed small, unsupported nanoparticles of both Cu and ZnO and showed up to 85% of the activity, in a squalane suspension, of the ternary reference.[11i] Other alkyl zinc alkoxides were also shown to undergo thermolysis in the presence of amine surfactants to yield quasi-homogeneous ZnO nanoparticles.[11k]

Subsequently, Fischer and co-workers reduced Cu/Zn stearate mixtures with hydrogen gas to produce copper nanoparticles, stabilized by zinc stearate.[11n]

Our group has focused on CO_2 rather than syn-gas as the carbon source. An alternative zinc oxide synthesis involving the hydrolysis of diethyl zinc, in the presence of substoichiometric quantities of zinc carboxylates/phosphinates produces 3−5 nm ZnO nanoparticles which are soluble in various organic solvents/polymers.[14] A high-activity carbon dioxide hydrogenation catalyst system was prepared by combining solutions of ZnO nanoparticles, surface coordinated by di(octyl)-phosphinate groups, with copper nanoparticles, surface-coordinated with stearate groups.[15] However, the optimum composition and nature of the precatalyst solution remains under-investigated. Furthermore, uncovering the relative importance of particle sizes, oxidation states of the metals, and interfaces between particles are central to improving catalytic activity. One drawback of this system is the requirement to pre-prepare separate solutions of the nano-particles. A "one-pot" method to prepare the catalyst would be desirable, as would be the replacement of hydrazine as the reductant in the preparation of copper nanoparticles. This paper presents a "one-pot" approach to catalyst synthesis, applying diethyl zinc as both the reductant to produce copper nanoparticles and the precursor to zinc oxide (by hydrolysis of Zn−C bonds). This method provides highly active carbon dioxide reduction catalysts, and through characterization of the pre- and postcatalyst solutions, the effects of organometallic precursor compound, relative loading, and metal oxidation state can be explored.

■ RESULTS AND DISCUSSION

Precatalyst Synthesis and Characterization. An in situ, one-pot catalyst preparation method that involved mixing together equimolar quantities of copper(II) bis(stearate) and diethyl zinc in toluene at 298 K (Scheme 1) was discovered. This solution showed several color changes consistent with the reduction of the copper(II) precursor and formation of a red/brown solution and characteristic of Cu(0) nanoparticles. It is proposed that ligand exchange occurs between the copper and zinc complexes, leading to transient formation of copper−alkyl species which are known to undergo rapid decomposition at room temperature to produce copper(0) species.[16] Ligand exchange would also be expected to lead to the formation of some zinc carboxylate species; such species have recently been shown to react with any excess dialkyl zinc to form heteroleptic alkyl zinc carboxylate complexes.[14b,d] The characterization data (vide infra) support this proposed ligand exchange and indicate the reaction proceeds to the formation of a solution containing copper(0) nanoparticles and well-defined zinc organometallic complexes.

The UV−vis spectrum of the red solution confirmed the formation of copper nanoparticles, with a copper surface plasmon absorbance observed at 580 nm (Figure S1).[17] The spectrum also clearly indicated the complete consumption of the Cu(II) precursor complex, as shown by the disappearance of its characteristic absorbance at 700 nm.

The speciation of the zinc was revealed by ^{1}H NMR spectroscopy (Figure S2), which showed the complete consumption of the paramagnetic species (e.g., Cu(II)) and the formation of well resolved signals consistent with the presence of diethyl zinc and an ethyl zinc stearate cluster compound, $Zn_5Et_4(stearate)_6$, the structure of which has been reported previously.[14b,d] The pentanuclear zinc cluster compound is known to form by reaction between diethyl zinc and bis(stearate)zinc and to retain its structure in noncoordinating solvent solutions.[14b,d] Analysis of the peak integrals in the ^{1}H NMR spectrum revealed a 3:2 molar ratio of $Et_2Zn/[Et_4Zn_5(stearate)_6]$ (Figure S2). We have also previously established that the hydrolysis of mixtures of diethyl zinc and the zinc stearate cluster, at analogous molar loadings, leads to the efficient formation of 3−5 nm zinc oxide nanoparticles, capped with stearate ligands.[14c]

The precatalyst solution was also analyzed by XAFS measurements, conducted in toluene solutions, under an inert atmosphere. The copper speciation was studied (Figure 1) by
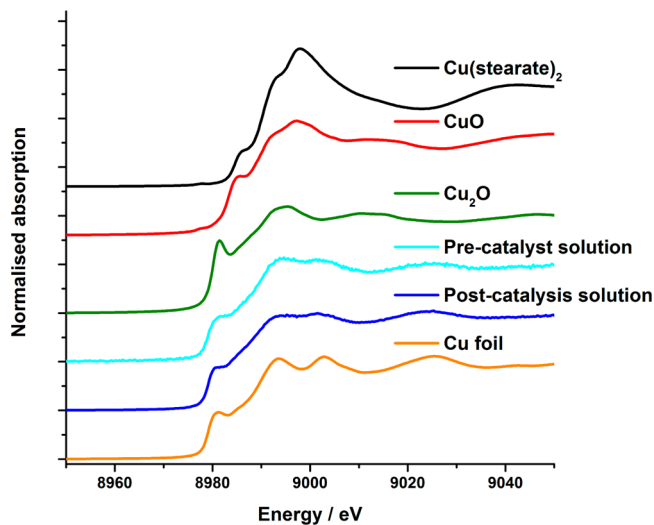

Figure 1. Normalized XANES spectra of Cu(stearate)$_2$ (black), CuO (red), Cu$_2$O (green), the precatalyst solution (light blue), the post catalysis solution (blue), and Cu foil (yellow).

comparing the Cu K-edge X-ray absorption near edge structure (XANES) spectra of the catalyst colloids with appropriate reference compounds, including Cu(stearate)$_2$, CuO, Cu$_2$O, and Cu metal. The precatalyst solution spectrum shows features similar to the Cu foil reference, implying the presence of metallic copper. Moreover, the XANES spectra lack any features typically associated with oxidic forms of Cu, primarily the peak at 8983.5 eV, indicative of linear Cu$_2$O (1s → 4p$_{x,y}$), and the peak at 8986.5 eV, which is evidence for CuO (1s → 4p$_z$).[18a] The main edge peaks are less well resolved than those of the copper foil, likely due to the nanoparticle size. Theoretical XANES simulations and experimental measurements of copper clusters have shown related effects, attributed to the absence of higher coordination shells and to a reduced particle size.[18]

The EXAFS data and calculated fitting parameters are evidence of the formation of copper nanoparticles and are illustrated in Figure S3 and Table S1. These data also indicate that the precatalyst solution contains small copper nanoparticles, again with no evidence for the formation of either of the oxides. The first-shell Cu−Cu coordination number can be used to estimate the particle size, according to the method developed by Beale et al.[19] The estimated mean particle size, from the EXAFS data, is 1.2 nm, consistent with the plasmon absorption observed in the UV−vis spectrum.[20]

The zinc XANES spectrum (Figure 2) of the precatalyst solution shows features in the absorption edge that are
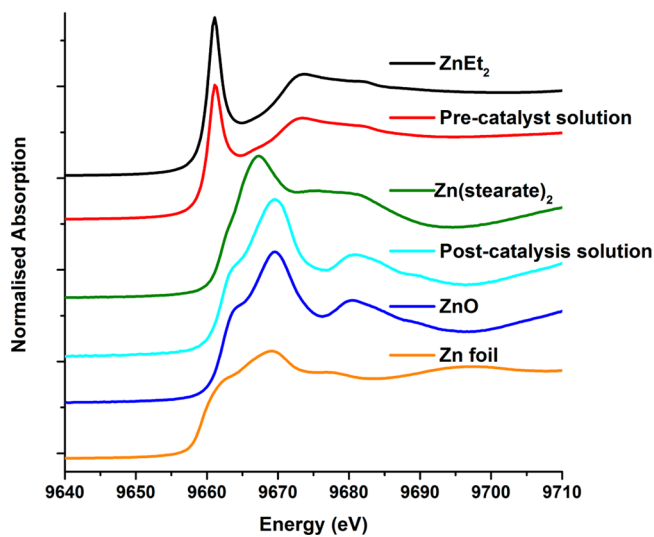

Figure 2. Normalized XANES spectra of diethyl zinc (black), the precatalyst solution (red), Zn(stearate)$_2$ (green), the post catalysis solution (light blue), ZnO nanoparticles with stearate capping groups (dark blue), and Zn foil (yellow).

consistent with the presence of both bis(stearate) zinc and diethyl zinc. A linear combination fit of the XANES data was calculated using Zn(stearate)$_2$ and diethyl zinc as reference compounds (Figure S4). A reasonable fit was obtained, having an R factor of 0.0025, based on a composition of ∼84% diethyl zinc and ∼16% Zn(stearate)$_2$. This estimation shows close agreement with the relative ratio of ethyl/stearate groups determined by analysis of the integrals for Et$_2$Zn and Et$_4$Zn$_5$(stearate)$_6$ in the ^{1}H NMR spectrum (∼86% of signals are due to zinc bound ethyl groups; ∼14% of signals, to zinc bound stearate moieties). It is apparent that the anaerobic techniques were sufficiently robust because the organozinc carboxylate cluster compound (Et$_4$Zn$_5$(stearate)$_6$) was successfully detected, a compound that is known to hydrolyze readily in the presence moisture.[14b,d] Furthermore, the zinc carbon bond lengths determined by the fits to the EXAFS data are in good agreement with those obtained for a sample of diethyl zinc (Table S2, Figure S5), providing good support for the presence of zinc−ethyl moieties in the precatalyst solution. The large Debye−Waller factor, compared with diethyl zinc, is also indicative of other species having Zn−C or Zn−O bonds, as would be expected from the ethyl zinc stearate cluster compound.

X-ray diffraction measurements were conducted on the precatalyst solution (after removal of all volatiles including diethyl zinc) (Figure S6). The samples are only weakly

Table 1. Effect of Varying the Weight Ratio ZnO/Cu on the Catalytic Activity for Carbon Dioxide Hydrogenation to Methanol[b]

entry	molar ratio precursors: $ZnEt_2$/Cu(stearate)$_2$	expected weight ratio ZnO/Cu	methanol peak activity, mmol g_{ZnOCu}^{-1} h^{-1}	methanol activity after 12 h, mmol g_{ZnOCu}^{-1} h^{-1}
1	1:3	30:70	39	39
2	1:1	55:45	60	58
3	2:1	70:30	43	37
4	7:1	90:10	18	13
5	ternary benchmark[a] (expected weight ratio of ZnO/Cu is 1:2)		60	46

[a]Alfa Aesar ternary methanol synthesis catalyst (product code: 45776), comprising (by weight) 24.7% ZnO, 63.5% CuO, 11.4% Al_2O_3, and MgO; see ESI for catalyst preactivation details and activity calculations. Error for each measurement is $\pm$4.5% as determined by runs in triplicate. Figures S7 and S8 illustrate the stability of the catalysts showing activity vs time. [b]Reaction conditions: 523 K, 50 bar (3:1, H_2/CO_2), in a solution of squalane/toluene (90:10) at a fixed total volume of 100 mL, a total gas flow of 166 mL min^{-1}, over 16 h. The total catalyst concentration (ZnO + Cu) was constant at 0.20 g dm^{-3}.

diffracting, but do confirm the presence of crystalline Cu metal. Some oxidation peaks (for CuO and Cu_2O) are observed, likely as a result of air exposure during sample preparation and measurement. The average copper particle size, determined for the Cu (111) peak using the Scherrer equation, is 4.8 nm, somewhat larger than the value obtained by EXAFS. However, EXAFS is more sensitive to detection of smaller clusters and particles, and XRD is volume-weighted to larger particles; therefore, a difference in the obtained particle size between the two measurements is to be expected in a polydisperse system. The XRD measurements also showed additional peaks at low angle, which correspond to signals expected for zinc-bound stearate groups, consistent with the presence of the ethyl zinc stearate cluster.

The combined spectroscopic data, therefore, indicate that the red precatalyst solution contains a mixture of 1−5 nm copper nanoparticles, presumably surface-capped with stearate ligands, and a mixture of diethyl zinc and ethyl zinc stearate clusters. Britten and co-workers have previously studied the reaction between diethyl zinc and Cu(II) precursors.[16] They established that diethyl zinc rapidly and irreversibly reduced the Cu(II) species to Cu, which formed as a mirror. This reaction was attributed to rapid ligand exchange and the instability of the resulting copper alkyl complexes, which underwent decomposition even at very low temperatures, purportedly by one-electron/radical processes. In the present case, the mechanisms are proposed to be similar, with the stearate ligands capping the nanoparticles and preventing copper mirror formation.

Carbon Dioxide Hydrogenation Catalysis. *Catalyst Composition.* The precatalyst solution was injected into a degassed solution of squalane in a continuously stirred tank reactor (CSTR), under an atmosphere of N_2 at 298 K. A 3:1 H_2/CO_2 mixture, at 50 bar, was added, and the reactor was heated to 523 K. The reaction was monitored using an in-line GC to detect the formation of methanol. During the first 120 min, the quantity of methanol produced steadily increased (a phenomenon partly resulting from reactor parameters, which introduce a delay in methanol detection by the GC instrument), reaching a steady state after ~2 h and remaining at this level for the duration of each experiment (12 h). Initially, ethane was also detected, but production ceased by 5 h (Figure S7). It is proposed that the ethane evolution results from the reaction of zinc ethyl groups in the precatalyst with water, which either is formed by carbon dioxide hydrogenation or is present in sufficient quantities in the gases/solvents. Indeed, a control experiment in which the precatalyst solution was exposed only to a continuous nitrogen flow in the reactor also resulted in ethane evolution over 5 h, after which time the

introduction of the reaction gases (CO_2/H_2) resulted in a catalyst system showing equivalent activity. Regardless of the source of the moisture, the hydrolysis reaction is expected to generate the ZnO nanoparticles, which in combination with the copper nanoparticles comprise the active catalyst (vide infra).

The method was applied to prepare a series of precatalyst solutions, using different molar ratios of diethyl zinc/copper-(stearate)$_2$ precursors, while keeping the overall loading of metals constant. The catalytic activities were benchmarked against the total mass of Cu and ZnO present, deduced from the molar quantities of the precursors and assuming complete conversions. The activities obtained using the precatalyst solutions were high and also very reproducible. For example, when a 1:1 molar mixture of diethyl zinc and copper stearate (55:45 weight ratio of ZnO/Cu) was applied, a methanol activity of 60 mmol g_{ZnOCu}^{-1} h^{-1} (133 mmol g_{Cu}^{-1} h^{-1}) was obtained (Table 1, Figure S7). This activity is similar to that obtained using a heterogeneous ternary syn-gas catalyst (preactivated according to the standard protocols)[21] as a benchmark material; however, after 10 h, the best catalyst system showed activity superior to the ternary heterogeneous catalyst control. These findings underscore the stability of the colloidal catalyst because the peak activity does not diminish significantly over the run (12 h), unlike the reference system.

It is clear that activity is strongly dependent on the relative quantities of zinc oxide and copper, at a fixed overall metal concentration (Figure S8). Optimum activities were observed for a 1:1 molar ratio of $ZnEt_2$/Cu(stearate)$_2$ precursors, which corresponds to an expected weight ratio of 55:45 ZnO/Cu, assuming complete conversions to the relevant oxide/metal nanoparticles (as indicated by the spectroscopic data). The activity rapidly decreased when either an excess of diethyl zinc (therefore, an increase in the ZnO loading) or an excess of copper stearate was applied. On one hand, sufficient diethyl zinc is required to reduce the copper completely; on the other hand, sufficient stearate (initially coordinated to the copper precursor) is required for nanoparticle stabilization. The colloidal nanoparticle catalysts show good stability over 12 h of the run, with activities remaining at or only slightly lower than the peak value for the duration of the run in the best case. In contrast, the ternary heterogeneous suspension shows a significant loss in activity after 12 h on-stream. Furthermore, in cases where an excess of diethyl zinc is added, significant deactivation is also observed. This is tentatively attributed to a reduction in the stability of the colloidal particles due to the reduced amount of stearate capping ligand available to stabilize the particles.

Catalyst Concentration. The influence of overall nano-particle concentration in the reactor was investigated at the optimum ratio of ZnO/Cu, 55:45 (1:1, Et$_2$Zn/Cu(stearate)$_2$) (Figure 3 and Table S3). As the nanoparticle concentration
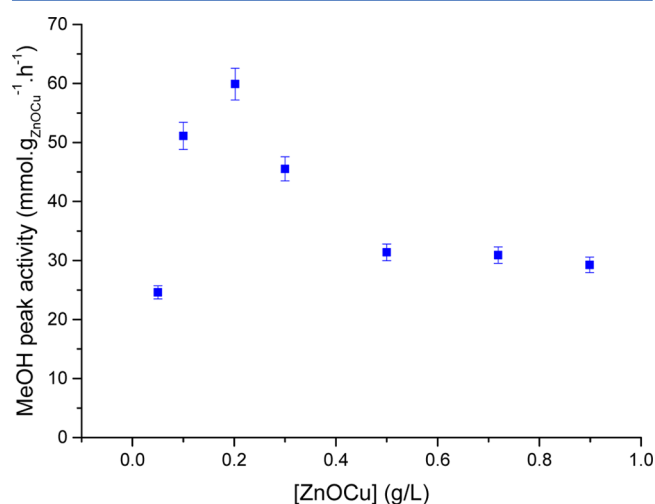

Figure 3. Influence of the overall catalyst concentration (ZnO + Cu in g$_{ZnOCu}$/L) on the methanol synthesis activity (mmol g$_{ZnOCu}^{-1}$ h^{-1}). The error for each measurement is ±4.5% as determined by runs in triplicate. The complete data set is presented in Table S3, and plots for each concentration of activity vs time are presented in Figure S9.

increases from 0 to 0.2 g$_{ZnOCu}$/L, the activity also steadily increases, presumably as the probability of an interaction between particles increases, allowing the formation of a catalytically active interface between ZnO and Cu. However, at nanoparticle concentrations above 0.2 g$_{ZnOCu}$/L, the activity decreases. At the relatively higher concentrations, aggregation of the nanoparticles appears to increase, presumably reducing the availability of active sites (which must be on the catalyst surface) and thereby reducing activity.[22]

Influence of the Organometallic Precursor Complexes. Various copper(II) and di(organo)zinc precursor complexes were investigated to establish the generality of the protocol to synthesize the catalyst (Table 2, Figure S10). All the complexes resulted in the formation of effective catalysts for methanol synthesis, with the activity depending weakly on the

Table 2. Influence of the Organometallic Precursor Complexes on Methanol Catalytic Activity[a]

copper precursor	zinc precursor	methanol peak activity, mmol g$_{ZnOCu}^{-1}$h^{-1}
Cu(stearate)$_2$	ZnEt$_2$	42
Cu(stearate)$_2$	ZnPh$_2$	32
Cu(laurate)$_2$	ZnEt$_2$	43
Cu(octanoate)$_2$	ZnEt$_2$	44
Cu(2-ethyl hexanoate)$_2$	ZnEt$_2$	39
Cu(dioctyl phosphinate)$_2$	ZnEt$_2$	50

[a]Reaction conditions: 523 K, 50 bar (3:1, H$_2$/CO$_2$), in squalane/toluene (90:10) at a fixed total volume of 100 mL, a total gas flow of 166 mL min^{-1}, over 16 h. The weight ratio of ZnO/Cu was fixed at 55:45, assuming complete conversion of the precursor complexes, and the overall catalyst concentration (ZnO + Cu) was fixed at 0.4 g$_{ZnOCu}$/L. Error for each measurement is 4.5% as determined by runs in triplicate. Figure S10 shows the activity vs time data for all catalysts.

nature of the precursor. In all cases, the catalysts operated in the same manner, with the evolution of ethane and formation of methanol over the first 5 h, followed by a steady state methanol production that does not significantly decrease over the following 12 h (Figure S10). Substituting diethyl zinc with diphenyl zinc, using bis(stearate) copper(II) as the copper source reduced the catalytic activity by ~25%. This reduction is tentatively attributed to differences in the reactivity of diphenyl zinc, both toward the Cu(II) precursor and toward water during the formation of zinc oxide in the reactor.

The influence of the copper precursor on catalytic activity, using diethyl zinc as the zinc oxide source, was more subtle. Using bis(laurate) or bis(octanoate) copper(II) precursors resulted in slightly more active catalysts than using bis(stearate) copper(II). It is likely that this effect relates to the balance between optimum solubility of the nanoparticles and steric hindrance and protection of the surface active sites. Thus, the optimum C-chain length for these carboxylate capped nano-particles appears to be 8 (octanoate).

We have previously reported a catalyst system prepared by mixing solutions of preformed nanoparticles of ZnO/Cu.[15] In that system, it was observed that increasing the reductive stability of the zinc oxide nanoparticle capping ligand by substituting carboxylate for di(octyl)phosphinate resulted in increased catalytic activity.[15] In this study, changing the copper precursor to di(octyl)phosphinate has a much lesser influence on activity, resulting in only a small increase. The Et$_2$Zn/Cu(di(octyl)phosphinate)$_2$ system was also tested at the 0.2 g$_{ZnOCu}$/L catalyst concentration (optimum for stearate), resulting in a peak activity of 60 mmol g$_{ZnOCu}^{-1}$ h^{-1}, which is close to the value for the Cu(stearate)$_2$ precursor (Figure S11).

Characterization. The optimum precatalyst solution was formed by the in situ reduction of copper stearate/phosphinate complexes with diethyl zinc. TEM analysis showed small nanoparticles (5−10 nm in diameter) in agglomerates containing from two to hundreds of nanoparticles (Figure 4). Some agglomeration is likely to occur during the catalyst precipitation, washing, and deposition required for TEM sample preparation, but the primary nanoparticles do appear to be intrinsically fused to form small clusters (Figure 4). Measurements of the lattice spacings in the high-resolution TEM images reveal that the nanoparticles consist of ZnO, Cu^0, and Cu$_2$O (Figure 4). Some nanoparticles showed a spacing of only ~2.47 Å, which corresponds to either ZnO(101) or Cu$_2$O(111). Such nanoparticles cannot be identified unambiguously. A lattice is not resolved in the remaining unidentified nanoparticles. Phases with larger lattice spacings are easier to resolve and, hence, easier to identify. ZnO(100) corresponds to a spacing 35% larger than Cu(111), which may be why the concentration of ZnO appears higher.

The high-resolution imaging was performed using an environmental TEM holder that prevented any exposure of the sample to air. Although the direct oxidation of Cu^0 to Cu$_2$O by water or CO$_2$ is unlikely, dissociative adsorption of CO$_2$ onto Cu^0, interacting with ZnO or other promoters, has been frequently reported[23] to form Cu$_2$O. Nevertheless, it is possible that trace O$_2$ during the washing sample preparation could also contribute to Cu oxidation. HAADF STEM−EDX further confirms that Cu-, Zn-, and O-containing nanoparticles are in close proximity (Figure S12). Intimate interaction between the copper and zinc oxide surfaces is thought to be important for highly active methanol synthesis catalysts[5c,7,24] and should be encouraged by the formation of zinc oxide in situ with the
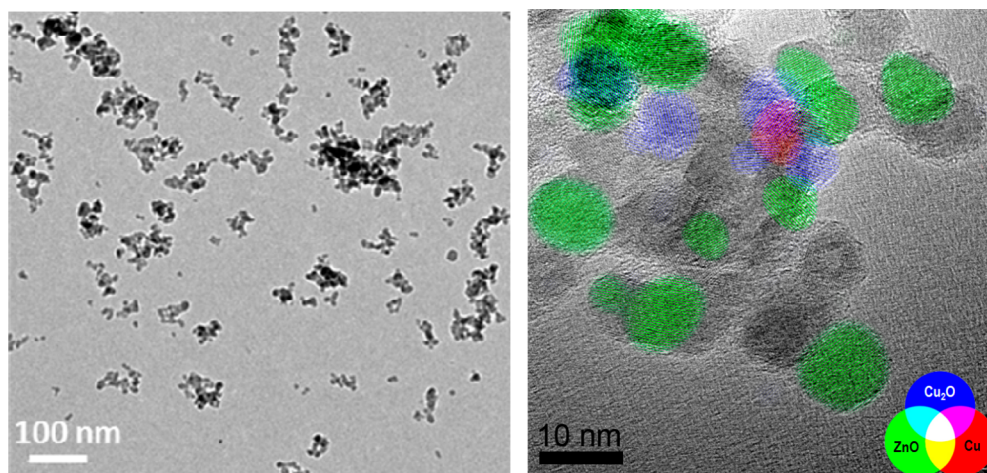
Figure 4. TEM images of the catalyst postreaction. (left) Low-resolution TEM image of discrete nanostructures. (right) High-resolution image of a nanoparticle cluster containing ZnO, Cu, and Cu_2O; colors indicate the phase where unambiguously identified by lattice analysis. Catalysis conditions: 1:1 $ZnEt_2$/$Cu(stearate)_2$ at fixed concentration (0.2 g dm^{-3}), 523 K, 50 bar (3:1, H_2/CO_2), in squalane at a fixed total volume of 100 mL, a total gas flow of 166 mLmin^{-1}, over 16 h.

copper nanoparticles. The presence of a contact interface between Cu-containing and ZnO nanoparticles is clearly observed in Figure 4.

The Zn K-edge XANES spectrum of the postcatalysis solution (Figure 2) also indicates that ZnO is present. The main edge peak observed at 9669 eV and a feature at 9663 eV are entirely consistent with the 1s → $4p_{x,y}$ and the 1s → $4p_z$ transitions of ZnO.[25] The Cu K-edge XANES spectrum of the same postcatalysis mixture indicates that the major copper-containing species continue to be Cu(0) nanoparticles (Figure 1). Indeed, the spectrum is essentially the same as that for the precatalysis mixture. On the other hand, the EXAFS data for the postcatalysis copper species demonstrate a small component of oxidic Cu species (as evidenced by the feature at ~1.8 Å in the Fourier transform data) as well as the Cu(0) species. The distance (1.84 Å) is consistent with a Cu(I)−O bond length, suggesting there may be minor contamination by Cu_2O in the postcatalysis sample (Figure S3, Table S1), consistent with the TEM observations. The EXAFS also shows features at R > 3 Å, which are indicative of metallic Cu. These features are more pronounced compared with the precatalysis mixture, likely due to an increase in nanoparticle size after catalysis; however, because of the mixed speciation of the copper postcatalysis, it is not possible to accurately quantify the copper nanoparticle size.

Powder X-ray diffraction measurements, conducted on the samples after centrifugation, also confirmed the presence of ZnO and copper nanoparticles in the postreaction mixtures. Figures S13−S15 illustrate the XRD patterns obtained for different loadings of ZnO/Cu; an illustrative example at 55:45 ZnO/Cu is shown in Figure 5. In every case, there are clearly peaks that can be indexed against the patterns expected for ZnO and copper nanoparticles. In most spectra, some copper oxidic species are also present (both Cu_2O and CuO), although the oxidation is proposed to occur predominantly during sample preparation, because the quantities present differ nonuniformly, and in one case, these species are absent (30:70, ZnO/Cu). The Scherrer equation can be used to estimate the relative particle sizes, and Table S4 lists these values for the various different loadings. In all cases, ~7 nm ZnO nanoparticles are estimated; on the other hand, the size of
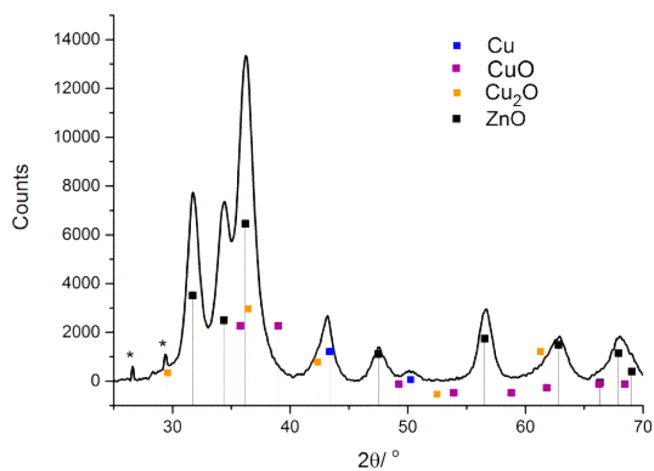

Figure 5. XRD of postcatalysis material for 55:45 ZnO/Cu (Table 1, entry 2). The spectrum is referenced to Cu (PDF no. 01-0851326 ICDD), Cu_2O (PDF no. 034-1354 ICDD), CuO (PDF no. 045-0937 ICDD), and ZnO (PDF no. 36-1451, ICDD).

the Cu particles appears rather more variable with low loadings of either ZnO/Cu (relating to lower molar quantities of either Et_2Zn or $Cu(stearate)_2$), resulting in the formation of significantly larger copper nanoparticles (~12−15 nm). When the relative loading of ZnO/Cu is more closely balanced (e.g., 55:45), then the sizes of the nanoparticles are also close, both being ~7 nm. This value is slightly higher than in the precatalyst solution, in line with the TEM images. It is tentatively proposed that the matching between the ZnO and Cu nanoparticle sizes may in part rationalize the improved activity shown at these loadings, possibly by maximizing the active interface between the two components.

■ CONCLUSIONS

Highly active, quasi-homogeneous CO_2 hydrogenation catalysts were produced by reaction between discrete inorganic complexes, namely, bis(carboxylate) copper(II) and diethyl zinc, to form precatalyst solutions. These solutions were applied (at 523 K, 50 bar of a 1:3 mixture of CO_2/H_2) to produce methanol in a continuously stirred slurry reactor

(squalane) with in-line GC detection equipment. The pre- and postcatalysis solutions were characterized using UV−vis, EXAFS, and XANES spectroscopy; microscopy (TEM); and, where possible, by ^{1}H NMR spectroscopy. The combined techniques indicate that the precatalysis mixture contains small (1−4 nm) copper nanoparticles and organometallic zinc complexes (diethyl zinc and ethyl zinc stearate cluster). On the other hand, after catalysis, the organozinc reagents were hydrolyzed to produce zinc oxide nanoparticles and the copper nanoparticles of sizes <10 nm. These spectroscopic findings are in line with ethane evolution (consistent with ethyl−zinc bond hydrolysis) during the initial phase of catalysis. The catalyst synthesis method was easily tuned, and the influence of the relative loadings of ZnO/Cu, the nature of the precursor compounds, and the effect of overall catalyst concentration were reported.

The best systems, which were formed using equimolar ratios of diethyl zinc/bis(stearate) copper in dry toluene gave activities for methanol production equivalent to those observed with a commercially available heterogeneous catalyst benchmark (mostly comprising ZnO, CuO, and Al$_2$O$_3$ mixtures). Thus, it is clear that formation of the copper nanoparticles, by reduction with diethyl zinc and subsequent in situ hydrolysis of the organozinc complexes results in a highly active and selective catalyst mixture. It is tentatively proposed that this increased activity may result from a preferential formation of ZnO/Cu interfaces using the in situ methodology (as compared with mixing together discrete solutions of nanoparticles). The facility with which variables can be changed as well as the ease of catalyst preparation make this route a rather attractive method for further optimization and investigation. In contrast to other (high temperature) methods to prepare Cu/ZnO particles, this synthesis operates at room temperature in organic solvents and yields highly reproducible, small nanoparticles surface-capped with organic ligands. Given the synthetic simplicity and potential to form nonequilibrium products, this method may well be applicable to a range of different catalytic systems, including those used for the production of methanol from synthesis gas.

■ ASSOCIATED CONTENT

ⓢ Supporting Information

The following file is available free of charge on the ACS Publications website at DOI: 10.1021/cs502038y.

Experimental details, 15 figures, 4 tables of results; additional references (PDF)

■ AUTHOR INFORMATION

Corresponding Authors

*E-mail: m.shaffer@imperial.ac.uk.
*E-mail: c.k.williams@imperial.ac.uk.

Notes

The authors declare no competing financial interest.

■ ACKNOWLEDGMENTS

■ REFERENCES

(1) (a) MacDowell, N.; Florin, N.; Buchard, A.; Hallett, J.; Galindo, A.; Jackson, G.; Adjiman, C. S.; Williams, C. K.; Shah, N.; Fennell, P. *Energy Environ. Sci.* **2010**, *3*, 1645−1669. (b) Kember, M. R.; Buchard, A.; Williams, C. K. *Chem. Commun.* **2011**, *47*, 141−163. (c) Aresta, M. *Carbon Dioxide as a Chemical Feedstock.* Wiley-VCH: Weinheim, 2010. (d) Darensbourg, D. J. *Inorg. Chem.* **2010**, *49*, 10765−10780. (e) Peters, M.; Köhler, B.; Kuckshinrichs, W.; Leitner, W.; Markewitz, P.; Müller, T. E. *ChemSusChem* **2011**, *4*, 1216−1240. (f) Wesselbaum, S.; vom Stein, T.; Klankermayer, J.; Leitner, W. *Angew. Chem., Int. Ed.* **2012**, *51*, 7499−7502. (g) Balaraman, E.; Gunanathan, C.; Zhang, J.; Shimon, L. J. W.; Milstein, D. *Nat. Chem.* **2011**, *3*, 609−614. (h) Menard, G.; Stephan, D. W. *J. Am. Chem. Soc.* **2010**, *132*, 1796−1797.

(2) Kondratenko, E. V.; Mul, G.; Baltrusaitis, J.; Larrazabal, G. O.; Perez-Ramirez, J. *Energy Environ. Sci.* **2013**, *6*, 3112−3135.

(3) (a) Olah, G. A. *Angew. Chem., Int. Ed.* **2013**, *52*, 104−107. (b) Pontzen, F.; Liebner, W.; Gronemann, V.; Rothaemel, M.; Ahlers, B. *Catal. Today* **2011**, *171*, 242−250. (c) Olah, G. A.; Goeppert, A.; Prakash, G. K. S. *J. Org. Chem.* **2009**, *74*, 487−498.

(4) Yang, C.-J.; Jackson, R. B. *Energy Policy* **2012**, *41*, 878−884.

(5) (a) Strunk, J.; Kähler, K.; Xia, X.; Muhler, M. *Surf. Sci.* **2009**, *603*, 1776−1783. (b) Baltes, C.; Vukojevic, S.; Schuth, F. *J. Catal.* **2008**, *258*, 334−344. (c) Behrens, M.; Studt, F.; Kasatkin, I.; Kuhl, S.; Havecker, M.; Abild-Pedersen, F.; Zander, S.; Girgsdies, F.; Kurr, P.; Kniep, B. L.; Tovar, M.; Fischer, R. W.; Norskov, J. K.; Schlogl, R. *Science* **2012**, *336*, 893−897. (d) Hansen, P. L.; Wagner, J. B.; Helveg, S.; Rostrup-Nielsen, J. R.; Clausen, B. S.; Topsoe, H. *Science* **2002**, *295*, 2053−2055. (e) Fichtl, M. B.; Schumann, J.; Kasatkin, I.; Jacobsen, N.; Behrens, M.; Schlögl, R.; Muhler, M.; Hinrichsen, O. *Angew. Chem., Int. Ed.* **2014**, *53*, 7043−7047.

(6) (a) Saito, M.; Murata, K. *Catal. Surv. Asia* **2004**, *8*, 285−294. (b) Saito, M.; Takeuchi, M.; Fujitani, T.; Toyir, J.; Luo, S. C.; Wu, J. G.; Mabuse, H.; Ushikoshi, K.; Mori, K.; Watanabe, T. *Appl. Organomet. Chem.* **2000**, *14*, 763−772. (c) Wang, W.; Wang, S. P.; Ma, X. B.; Gong, J. L. *Chem. Soc. Rev.* **2011**, *40*, 3703−3727. (d) Wu, J. G.; Saito, M.; Takeuchi, M.; Watanabe, T. *Appl. Catal., A* **2001**, *218*, 235−240. (e) Li, C.; Yuan, X.; Fujimoto, K. *Appl. Catal., A* **2014**, *469*, 306−311. (f) Natesakhawat, S.; Lekse, J. W.; Baltrus, J. P.; Ohodnicki, P. R.; Howard, B. H.; Deng, X. Y.; Matranga, C. *ACS Catal.* **2012**, *2*, 1667−1676. (g) Saito, M.; Fujitani, T.; Takeuchi, M.; Watanabe, T. *Appl. Catal., A* **1996**, *138*, 311−318. (h) Fisher, I. A.; Bell, A. T. *J. Catal.* **1997**, *172*, 222−237. (i) Liu, X. M.; Lu, G. Q.; Yan, Z. F.; Beltramini, J. *Ind. Eng. Chem. Res.* **2003**, *42*, 6518−6530. (j) Fujita, S.; Usui, M.; Ito, H.; Takezawa, N. *J. Catal.* **1995**, *157*, 403−413. (k) Koeppel, R. A.; Baiker, A.; Wokaun, A. *Appl. Catal., A* **1992**, *84*, 77−102. (l) Dutta, G.; Sokol, A. A.; Catlow, C. R. A.; Keal, T. W.; Sherwood, P. *ChemPhysChem* **2012**, *13*, 3453−3456. (m) Grabow, L. C.; Mavrikakis, M. *ACS Catal.* **2011**, *1*, 365−384.

(7) Behrens, M.; Schloegl, R. *Z. Anorg. Allg. Chem.* **2013**, *639*, 2683−2695.

(8) Weiss, R.; Guo, Y. Z.; Vukojevic, S.; Khodeir, L.; Boese, R.; Schuth, F.; Muhler, M.; Epple, M. *Eur. J. Inorg. Chem.* **2006**, 1796−1802.

(9) (a) Liao, F. L.; Huang, Y. Q.; Ge, J. W.; Zheng, W. R.; Tedsree, K.; Collier, P.; Hong, X. L.; Tsang, S. C. *Angew. Chem., Int. Ed.* **2011**, *50*, 2162−2165. (b) Liao, F. L.; Zeng, Z. Y.; Eley, C.; Lu, Q.; Hong, X. L.; Tsang, S. C. E. *Angew. Chem., Int. Ed.* **2012**, *51*, 5832−5836. (c) Zhou, X. W.; Qu, J.; Xu, F.; Hu, J. P.; Foord, J. S.; Zeng, Z. Y.; Hong, X. L.; Tsang, S. C. E. *Chem. Commun.* **2013**, *49*, 1747−1749.

(10) Lee, S. G.; Sardesai, A. *Top. Catal.* **2005**, *32*, 197−207.

(11) (a) Hambrock, J.; Rabe, S.; Merz, K.; Birkner, A.; Wohlfart, A.; Fischer, R. A.; Driess, M. *J. Mater. Chem.* **2003**, *13*, 1731−1736. (b) Hambrock, J.; Schroter, M. K.; Birkner, A.; Woll, C.; Fischer, R. A. *Chem. Mater.* **2003**, *15*, 4217−4222. (c) Lu, L. H.; Wohlfart, A.; Parala, H.; Birkner, A.; Fischer, R. A. *Chem. Commun.* **2003**, 40−41.

(d) Tkachenko, O. P.; Klementiev, K. V.; Loffler, E.; Ritzkopf, I.; Schuth, F.; Bandyopadhyay, M.; Grabowski, S.; Gies, H.; Hagen, V.; Muhler, M.; Lu, L. H.; Fischer, R. A.; Grunert, W. *Phys. Chem. Chem. Phys.* **2003**, *5*, 4325−4334. (e) Kurtz, M.; Bauer, N.; Buscher, C.; Wilmer, H.; Hinrichsen, O.; Becker, R.; Rabe, S.; Merz, K.; Driess, M.; Fischer, R. A.; Muhler, M. *Catal. Lett.* **2004**, *92*, 49−52. (f) Lu, L. H.; Fischer, R. A. *Chem. Lett.* **2004**, *33*, 1318−1319. (g) Cokoja, M.; Parala, H.; Schroter, M. K.; Birkner, A.; van den Berg, M. W. E.; Klementiev, K. V.; Grunert, W.; Fischer, R. A. *J. Mater. Chem.* **2006**, *16*, 2420−2428. (h) Schroeder, F.; Hermes, S.; Parala, H.; Hikov, T.; Muhler, M.; Fischer, R. A. *J. Mater. Chem.* **2006**, *16*, 3565−3574. (i) Schroter, M. K; Khodeir, L.; van den Berg, M. W. E.; Hikov, T.; Cokoja, M.; Miao, S. J.; Grunert, W.; Muhler, M.; Fischer, R. A. *Chem. Commun.* **2006**, 2498−2500. (j) Lu, L.; Hu, S.; Lee, H.-I.; Woell, C.; Fischer, R. A. *J. Nanoparticle Res.* **2007**, *9*, 491−496. (k) Hikov, T.; Rittermeier, A.; Luedemann, M.-B.; Herrmann, C.; Muhler, M.; Fischer, R. A. *J. Mater. Chem.* **2008**, *18*, 3325−3331. (l) Mueller, M.; Hermes, S.; Kaehler, K.; van den Berg, M. W. E.; Muhler, M.; Fischer, R. A. *Chem. Mater.* **2008**, *20*, 4576−4587. (m) Lee, B. H.; Hwang, J. K.; Nam, J. W.; Lee, S. U.; Kim, J. T.; Koo, S.-M.; Baunemann, A.; Fischer, R. A.; Sung, M. M. *Angew. Chem., Int. Ed.* **2009**, *48*, 4536−4539. (n) Rittermeier, A.; Miao, S.; Schroeter, M. K.; Zhang, X.; van den Berg, M. W. E.; Kundu, S.; Wang, Y.; Schimpf, S.; Loeffler, E.; Fischer, R. A.; Muhler, M. *Phys. Chem. Chem. Phys.* **2009**, *11*, 8358−8366. (o) Schimpf, S.; Rittermeier, A.; Zhang, X.; Li, Z.-A.; Spasova, M.; van den Berg, M. W. E.; Farle, M.; Wang, Y.; Fischer, R. A.; Muhler, M. *ChemCatChem* **2010**, *2*, 214−222. (p) Sliem, M. A.; Hikov, T.; Li, Z.-A.; Spasova, M.; Farle, M.; Schmidt, D. A.; Havenith-Newen, M.; Fischer, R. A. *Phys. Chem. Chem. Phys.* **2010**, *12*, 9858−9866. (q) Sliem, M. A.; Turner, S.; Heeskens, D.; Kalidindi, S. B.; Van Tendeloo, G.; Muhler, M.; Fischer, R. A. *Phys. Chem. Chem. Phys.* **2012**, *14*, 8170−8178. (r) Vukojevic, S.; Trapp, O.; Grunwaldt, J. D.; Kiener, C.; Schuth, F. *Angew. Chem., Int. Ed.* **2005**, *44*, 7978−7981.

(12) Simon, M.; Mortreux, A.; Petit, F. *J. Chem. Soc., Chem. Commun.* **1988**, 1445−1446.

(13) Corker, J. M.; Evans, J. *J. Chem. Soc., Chem. Commun.* **1994**, 1027−1029.

(14) (a) Gonzalez-Campo, A.; Orchard, K. L.; Sato, N.; Shaffer, M. S. P.; Williams, C. K. *Chem. Commun.* **2009**, 4034−4036. (b) Orchard, K. L.; Harris, J. E.; White, A. J. P.; Shaffer, M. S. P.; Williams, C. K. *Organometallics* **2011**, *30*, 2223−2229. (c) Orchard, K. L.; Shaffer, M. S. P.; Williams, C. K. *Chem. Mater.* **2012**, *24*, 2443−2448. (d) Orchard, K. L.; White, A. J. P.; Shaffer, M. S. P.; Williams, C. K. *Organometallics* **2009**, *28*, 5828−5832.

(15) Brown, N. J.; Weiner, J.; Hellgardt, K.; Shaffer, M. S. P.; Williams, C. K. *Chem. Commun.* **2013**, *49*, 11074−11076.

(16) (a) Vidjayacoumar, B.; Emslie, D. J. H.; Blackwell, J. M.; Clendenning, S. B.; Britten, J. F. *Chem. Mater.* **2010**, *22*, 4854−4866. (b) Vidjayacoumar, B.; Emslie, D. J. H.; Clendenning, S. B.; Blackwell, J. M.; Britten, J. F.; Rheingold, A. *Chem. Mater.* **2010**, *22*, 4844−4853.

(17) (a) Curtis, A. C.; Duff, D. G.; Edwards, P. P.; Jefferson, D. A.; Johnson, B. F. G.; Kirkland, A. I.; Wallace, A. S. *J. Phys. Chem.* **1988**, *92*, 2270−2275. (b) Papavassiliou, C.; Kokkinakis, T. *J. Phys. F: Met. Phys.* **1974**, *4*, L67.

(18) (a) Rothe, J.; Hormes, J.; Bonnemann, H.; Brijoux, W.; Siepen, K. *J. Am. Chem. Soc.* **1998**, *120*, 6019−6023. (b) Montano, P. A.; Shenoy, G. K.; Alp, E. E.; Schulze, W.; Urban, J. *Phys. Rev. Lett.* **1986**, *56*, 2076−2079.

(19) Beale, A. M.; Weckhuysen, B. M. *Phys. Chem. Chem. Phys.* **2010**, *12*, 5562−5574.

(20) Creighton, J. A.; Eadon, D. G. *J. Chem. Soc., Faraday Trans.* **1991**, *87*, 3881−3891.

(21) Sawant, A.; Ko, M. K.; Parameswaran, V.; Lee, S.; Kulik, C. *J. Fuel Sci. Technol.* **1987**, *5*, 77−88.

(22) (a) Selvam, N. C. S.; Narayanan, S.; Kennedy, L. J.; Vijaya, J. J. *J. Environ. Sci.* **2013**, *25*, 2157−2167. (b) Huang, M.; Xu, C.; Wu, Z.; Huang, Y.; Lin, J.; Wu, J. *Dyes Pigm.* **2008**, *77*, 327−334.

(23) (a) Fujitani, T.; Saito, M. *Catal. Lett.* **1994**, *25*, 271−276. (b) Yurieva, T. M.; Plyasova, L. M.; Makarova, O. V.; Krieger, T. A. *J. Mol. Catal. A: Chem.* **1996**, *113*, 455−468. (c) Chinchen, G. C.; Spencer, M. S.; Waugh, K. C.; Whan, D. A. *J. Chem. Soc., Faraday Trans.* **1987**, *83*, 2193−2212. (d) Chinchen, G. C.; Waugh, K. C.; Whan, D. A. *Appl. Catal.* **1986**, *25*, 101−107.

(24) (a) Behrens, M. *J. Catal.* **2009**, *267*, 24−29. (b) Behrens, M.; Zander, S.; Kurr, P.; Jacobsen, N.; Senker, J.; Koch, G.; Ressler, T.; Fischer, R. W.; Schlögl, R. *J. Am. Chem. Soc.* **2013**, *135*, 6061−6068.

(25) Grandjean, D.; Castricum, H. L.; Van Den Heuvel, J. C.; Weckhuysen, B. M. *J. Phys. Chem. B* **2006**, *110*, 16892−16901.